Electronic Supplementary Material (ESI) for ChemComm.

Electronic Supplementary Information

Proton-detected Solid-state NMR Detects the Inter-nucleotide Correlations and Architecture of Dimeric RNA in Microcrystals

Yufei Yang,[a,b,e] ShengQi Xiang,[c] Xiaodan Liu,[d] Xiaojing Pei,[a,e] Pengzhi Wu,[d] Qingguo Gong,[d] Na Li,[a,e] Marc Baldus,[c] and Shenlin Wang*[a,b,e]

[a] College of Chemistry and Molecular Engineering and [b] Beijing NMR Center, Peking University, Beijing, China

[c] NMR Spectroscopy, Bijvoet Center for Biomolecular Research, Utrecht University, Padualaan 8, 3584 CH Utrecht, The Netherlands

[d] Hefei National Laboratory for Physical Science at Microscale, Collaborative Innovation Center of Chemistry for Life Sciences and School of Life Sciences, University of Science and Technology of China, Hefei, Anhui, 230027, China

[e] Beijing National Laboratory for Molecular Sciences, Beijing, China

**Corresponding author. E-mail: wangshenlin@pku.edu.cn*

Materials and Methods

In vitro transcription reaction and purification of RNA

The ^{15}N, ^{13}C isotope-enriched NTPs were purchased from Cambridge Isotope Laboratories (Andover, MA). The commercial NTPs with natural abundance were purchased from Sangon Biotech (Shanghai, China). The common reagent grade chemicals were purchased from either Thermo Fisher Scientific or Sigma-Aldrich. The DNA templates for *in vitro* transcription reaction were purchased from BGI company (Beijing, China).

The 23-mer RNA (5′-GGGCUUGCUGAGGUGCACACAGCAAG-3′) from the HIV-1 dimerization initiation site (DIS-HIV-1 hereafter) was produced using an *in vitro* transcription reaction catalyzed by T7 RNA polymerase, as described elsewhere.[1] Two oligonucleotides with sequences of 5′-GAAATTAATACGACTCACTATAGGG-3′ and 5′-CTTGCTGTGTGCACCTCAGCAAGCCCTATAGTGAGTCGTATTAATTTC-3′ were annealed to form a DNA template. The DNA template with a final concentration of 0.3 μM

was added to 10 mL pH 7.0 reaction mixtures (40 mM Tris-HCl, 0.01% Triton X-100, 1 mM spermidine, 5 mM NTPs, 10 mM DTT, 0.1 mg/mL T7 RNA polymerase, and 50 mM $MgCl_2$). To produce the $^{15}N,^{13}C$-labeled RNA samples, the $^{15}N,^{13}C$-labeled NTPs replaced the corresponding naturally abundant NTPs. The *in vitro* transcription reaction mixtures were incubated at 37 ºC for 4 hours. The synthesized RNA was purified using polyacrylamide gel electrophoresis (PAGE) along with electroelution recovery. The final yield of the purified DIS-HIV-1 was 4 mg per 10 mL of reaction system.

Preparation of the DIS-HIV-1 dimer

In water, the purified DIS-HIV-1 is monomeric, whereas it forms homodimers in the presence of cations, i.e., Mg^{2+}, K^+, and spermidine (Fig. S1). Several buffer conditions and annealing protocols were screened to improve the yield of the dimeric species (Fig. S1).

To prepare the dimeric DIS-HIV-1, the purified sample was concentrated to ~10 mg/mL and annealed in a pH 7.0 buffer A (20 mM sodium cacodylate, 5 mM $MgCl_2$, 150 mM KCl, and 5 mM spermidine) by heating to 95 ºC for 3 min, followed by cooling down to room temperature and incubating at 37ºC for 2 hours before crystallization. For the isotopically diluted RNA sample, the isotope-labeled DIS-HIV-1 was mixed with an equal amount of naturally abundant DIS-HIV-1 in monomeric form, which was then annealed in buffer A to form the isotopically diluted dimeric DIS-HIV-1. 16% Native PAGE was used to monitor the purity and the oligomerization state of the DIS-HIV-1 (Fig. S1).

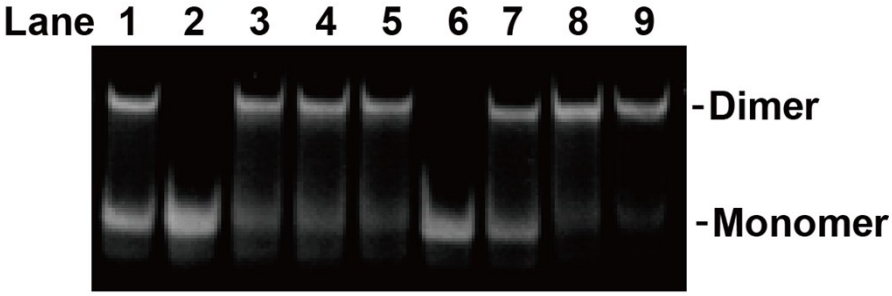

Fig. S1 Results of the 16% native PAGE used to characterize the aggregation state of DIS-HIV-1 in different buffer conditions. Lane 1: DIS-HIV-1 after the *in vitro* transcription reaction. Lane 2: DIS-HIV-1 is annealed in aqueous solution. Lanes 3-5: DIS-HIV-1 is annealed in pH 7.0 solution containing 5 mM Mg^{2+} (Land 3), 25 mM Mg^{2+} (Lane 4), and 50 mM Mg^{2+} (Lane 5). Lanes 6 and 7: DIS-HIV-1 is annealed in a pH 7.0 solution with 10 mM K^+ (Lane 6) and 150 mM K^+ (Lane 7). Lane 8: DIS-HIV-1 is annealed in pH 7.0 buffer with 10 mM spermidine. Lane 9: DIS-HIV-1 is annealed in pH 7.0 solution with 5 mM Mg^{2+}, 150 mM K^+, and 5 mM spermidine solution.

Sample preparation for SSNMR

We prepared three dimeric DIS-HIV-1 samples with different labeling schemes: (*i*) $^{15}N,^{13}C$-labeled guanosines and cytidines, $(G,C)^{Lab}$-RNA; (*ii*) $(G,C)^{Lab}$-RNA diluted with an equal amount of the naturally abundant RNA (NA-RNA) sample; and (*iii*) uniformly $^{15}N,^{13}C$-labeled $(G,C,A,U)^{Lab}$-RNA sample.

All of the DIS-HIV-1 samples were crystallized by batch methods, using a protocol adapted from the rapid bulk crystallization method for generating nanocrystalline protein and RNA samples.[2] As reported previously, the SSNMR spectral resolution of proteins in nanocrystallines is nearly identical to those in single crystals.[2] Thus we used the rapid crystallization protocol to prepare RNA nanocrystalline for SSNMR studies. The dimeric RNA samples were incubated at 37 ºC for 2 hours, followed by the addition of a precipitant solution (50 mM spermine and 10% methylpentanediol (MPD)) at a ratio of 10% (v/v) and an equal volume of reservoir solution (50% MPD, 50 mM sodium cacodylate, 100 mM $MgCl_2$, and 300 mM KCl). The RNA precipitation appeared rapidly and was collected after an overnight incubation at 4 ºC. However, the monomeric state could not be crystallized under above condition. The crystalline morphology of the DIS-HIV-1 was characterized by scanning electron microscopy (SEM, Hitachi S-4800 Field Emission Scanning Electron Microscope, Japan), using an electrical potential of 5.0 kV and a corresponding electrical current of 10 μA. Morphologically, the RNA crystallites had a broadly uniform square shape with calculated particle sizes ranging from 0.1 to 1 μm (Fig. S2).

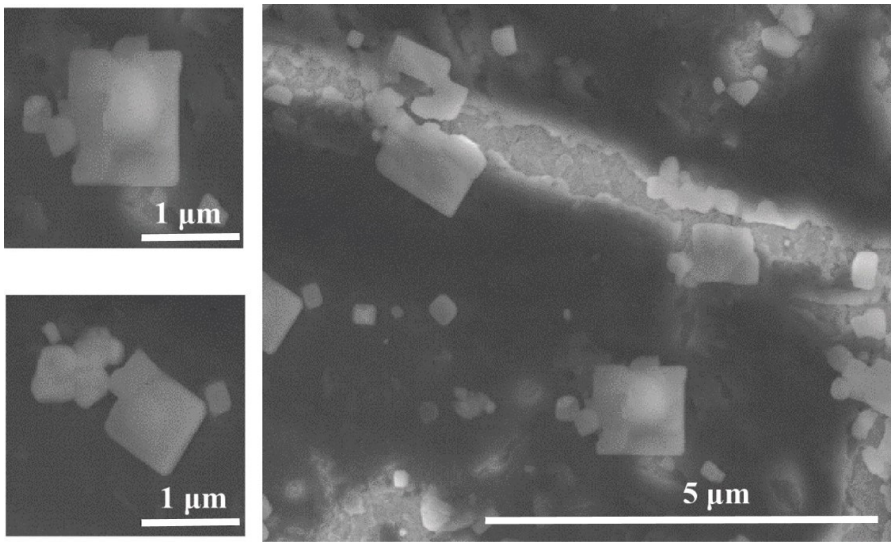

Fig. S2 SEM photo of the micro-crystallized DIS-HIV-1 produced using rapid batch crystallization.

MAS SSNMR spectroscopy

For each type of labelled sample, approximately 3 mg of the crystallized RNA sample was center-packed into a 1.9-mm SSNMR rotor by centrifugation. All of the SSNMR experiments were carried out on a Bruker Avance III spectrometer, operating at the proton frequency of 600.25 MHz. The spectrometer was equipped with a 1.9 mm triple-resonance ^{1}H-X-Y MAS probe with a magic-angle-spinning rate of 40 kHz. All of the experiments were carried at 5 ^{o}C to avoid the RNA degradation and minimize the conformational flexibility. Typical π/2 pulse lengths were 2.0 μs for ^{1}H, 4.0 μs for ^{13}C, and 5.0 μs for ^{15}N.

Both the HN-CP and the hN(PAR)N experiments were recorded with 1024 scans. Four types of the proton-detected 2D ^{1}H-^{15}N correlation experiments, hNH, hN(PAR)NH, hCNH, and hCN(PAR)NH were used, according to the pulse sequences shown in Fig. 3 of the manuscript and Fig. S3. A total of 300 and 1,024 points were acquired in t_1 and t_2, leading to total acquisition times of 15 and 20 ms, respectively. For all of the 2D experiments, low-power TPPM proton decoupling (nutation frequency ~10 kHz) was used during the evolution of the ^{15}N chemical shift,[3] and WALTZ-16 decoupling (nutation frequency ~15 kHz) on the ^{15}N channel was applied during the evolution of the proton chemical shift. The MISSISIPPI pulse trains were applied for water and MPD signal suppression.[4] The recycle delays of all SSNMR experiments were set to 2.0 s.

The pulse sequence for the 2D hNH experiment was adapted from previous protein studies using SSNMR.[4] Both the ^{1}H-^{15}N and the ^{15}N-^{1}H CP transfer were set with constant field lock of ^{15}N at 60 kHz and with the proton power ramped linearly around n=1 Hartmann–Hahn (HH) conditions.[5] The contact times for ^{1}H-^{15}N and ^{15}N-^{1}H CP were 4 ms and 300 μs, respectively. The hNH experiments were recorded with 16 scans.

The pulse sequence of the 2D hN(PAR)NH experiment was designed using blocks similar to those in the 2D hNH experiment, with an additional ^{15}N-^{15}N PAR transfer period following the ^{15}N chemical shift evolution.[6] The ^{1}H-^{15}N and the ^{15}N-^{1}H CP of the 2D hN(PAR)NH were identical to those in the hNH experiments. As for the ^{15}N-^{15}N PAR transfer, the contact time was 7 ms, with a constant lock field of 26 kHz and 67 kHz on the ^{15}N and ^{1}H channels, respectively. The phase cycle of the spin lock within the PAR period was set as (*y*, *-y*) for the ^{15}N channel and *y* for the ^{1}H channel (Fig. S3) to suppress the ^{1}H-^{15}N CP signals along with the PAR transfer. The hN(PAR)NH experiments were recorded with 32 scans.

For the 2D hCNH experiments, the initial ^{1}H-^{13}C CP contact time was 1.5 ms, with a constant lock field of 60 kHz on ^{13}C and a proton field ramped linearly around 100 kHz. The ^{13}C-^{15}N SPECIFIC CP transfers were implemented with a contact time of 5.5 ms,[7] with a

constant lock field of 15 kHz on ^{13}C and a ^{15}N lock field ramped linearly (10%) around 25 kHz (optimized experimentally). A continuous-wave proton decoupling of 100 kHz was applied during the ^{13}C-^{15}N CP transfer. The carrier frequencies were placed at 160 ppm for ^{13}C and 190 ppm for ^{15}N, respectively. The final ^{15}N-^{1}H CP transfer was identical to that of the hNH experiment. For the hCN(PAR)NH experiments, a ^{15}N-^{15}N PAR transfer step followed the evolution of the indirect chemical shift, with respect to the hCNH experiment. The parameters for the ^{15}N-^{15}N PAR of hCN(PAR)NH were identical to those of the hN(PAR)NH experiment. The hCNH and hCN(PAR)NH were recorded with 32 and 100 scans, respectively.

All of the NMR data processing was performed using TOPSPIN. The spectra were analyzed using CARA.[8] Chemical shifts were referenced to 2,2-dimethyl-2-silapentane-5-sulfonic acid (DSS), using adamantane as a secondary standard.[9] The ^{1}H and ^{15}N chemical shifts were referenced indirectly using $\gamma^{13}C/\gamma^{1}H = 0.25145020$ and $\gamma^{15}N/\gamma^{13}C = 0.40297994$, respectively.

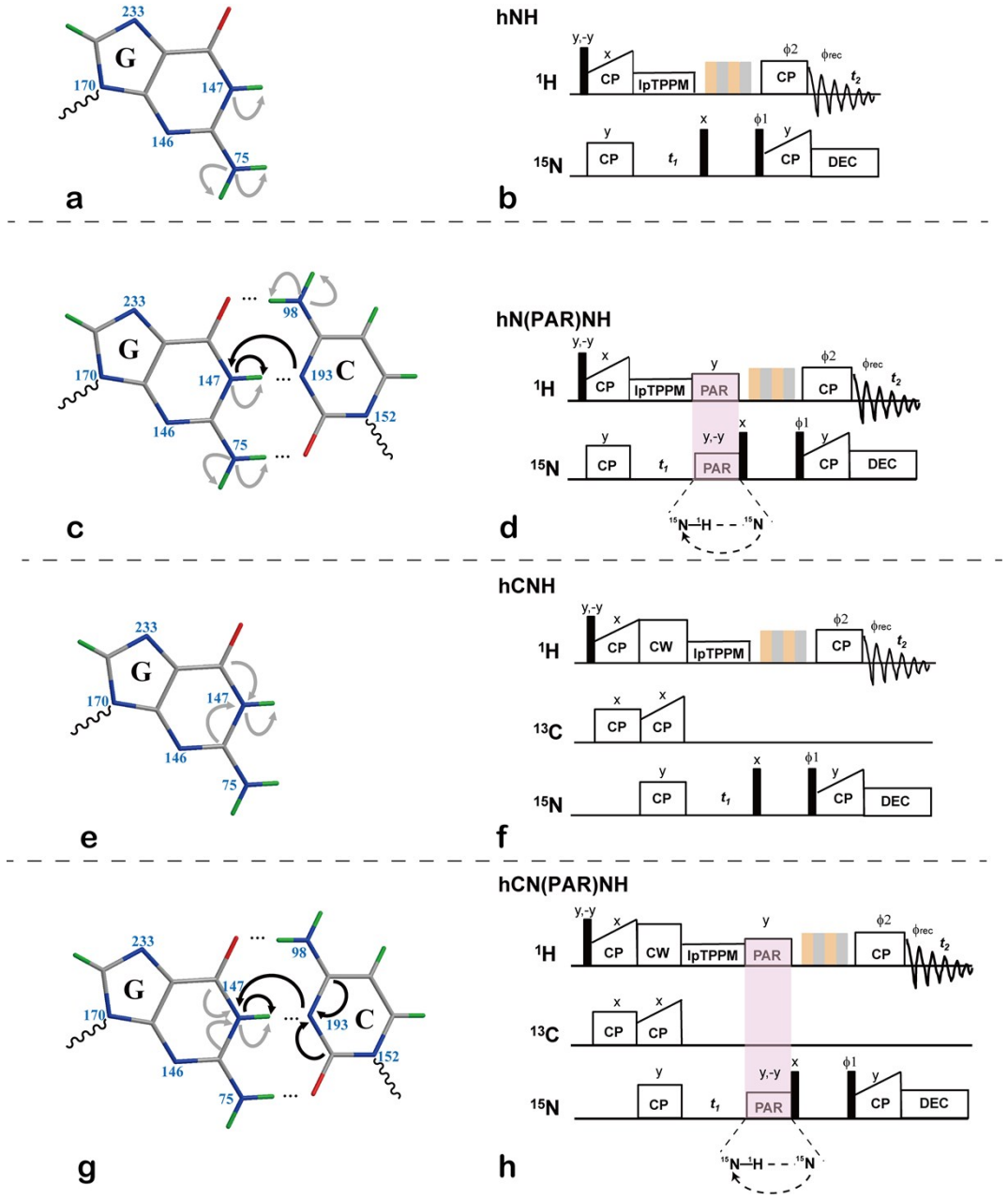

Fig. S3 Pulse sequences for the ^{1}H-detected ^{1}H-^{15}N chemical shift correlation experiments and schematic representations of the magnetization transfer pathways, shown on the chemical structures of guanosine and cytidine as examples. Pulse sequences and magnetization transfer pathways for a,b) the hNH experiments and e,f) the hCNH experiments. Pulse sequences and corresponding magnetization transfer pathways for c,d) the hN(PAR)NH experiments and g,h) the hCN(PAR)NH experiments. The black arrows show the inter-nucleotide transfers based on the ^{15}N-^{15}N PAR mechanisms, and the gray arrows indicate the intra-nucleotide correlations within the amino and the imino groups. In the hCNH and hCN(PAR)NH experiments, the ^{13}C-^{15}N SPECIFIC CP period selectively polarizes the ^{15}N nuclei with chemical shifts higher than 140 ppm, without exciting the amino groups. For all of the pulse sequences, filled black bars represent π/2 pulses. The phase cycles are indicated on the pulse sequences, except those for ϕ1 = (x, x, -x, -x), ϕ2 = (y, y, y, y, -y, -y, -y, -y), and ϕrec= (y, -y, -y, y, -y, y, y, -y). The yellow and gray bars represent the water suppression period using MISSISIPPI pulse trains.[4] The TPPI phase-sensitive detection was obtained in the indirect t_1 dimension by incrementing the first π/2 pulse of the ^{1}H channel.

Results and Discussion

Characterization of the Kissing-loop Structure of DIS-HIV-1

Verification of the kissing-loop structure of DIS-HIV-1 using RNA ligation reactions

We developed an RNA ligation strategy using T4 RNA ligase (New England Biolabs (Beijing) LTD.) to prove the kissing-loop structure of dimeric DIS-HIV-1. T4 RNA ligase is capable of catalyzing the ligation of a 5′ phosphoryl-terminated nucleic acid donor to a 3′ hydroxyl-terminated nucleic acceptor. It is expected that a kissing-loop structure would produce cyclic dimers, whereas an extended duplex structure would produce higher order multimers (Fig. S4).[10]

The reaction system, composed of 20 μL of dimeric DIS-HIV-1 (~ 4 μg), a ligation buffer, and T4 RNA ligase, was incubated at 37 ℃ overnight to complete the reaction. A control experiment on the RNA sample using identical conditions but without the addition of T4 RNA ligase was conducted to exclude the possibility that the RNA could ligate spontaneously to generate higher order multimers. After the ligation reaction, the products were investigated using a 16% denaturing PAGE technique (Fig. S4 c); the identified cyclic dimer and linear dimer indicated a kissing-loop structure, not the higher order multimers that would be produced by an extended duplex structure. The cyclic dimer migrates slightly faster than the linear dimer, and the latter product may be caused by incomplete ligation reactions. Thus our data proved that dimeric DIS-HIV-1 organizes into a kissing-loop structure.

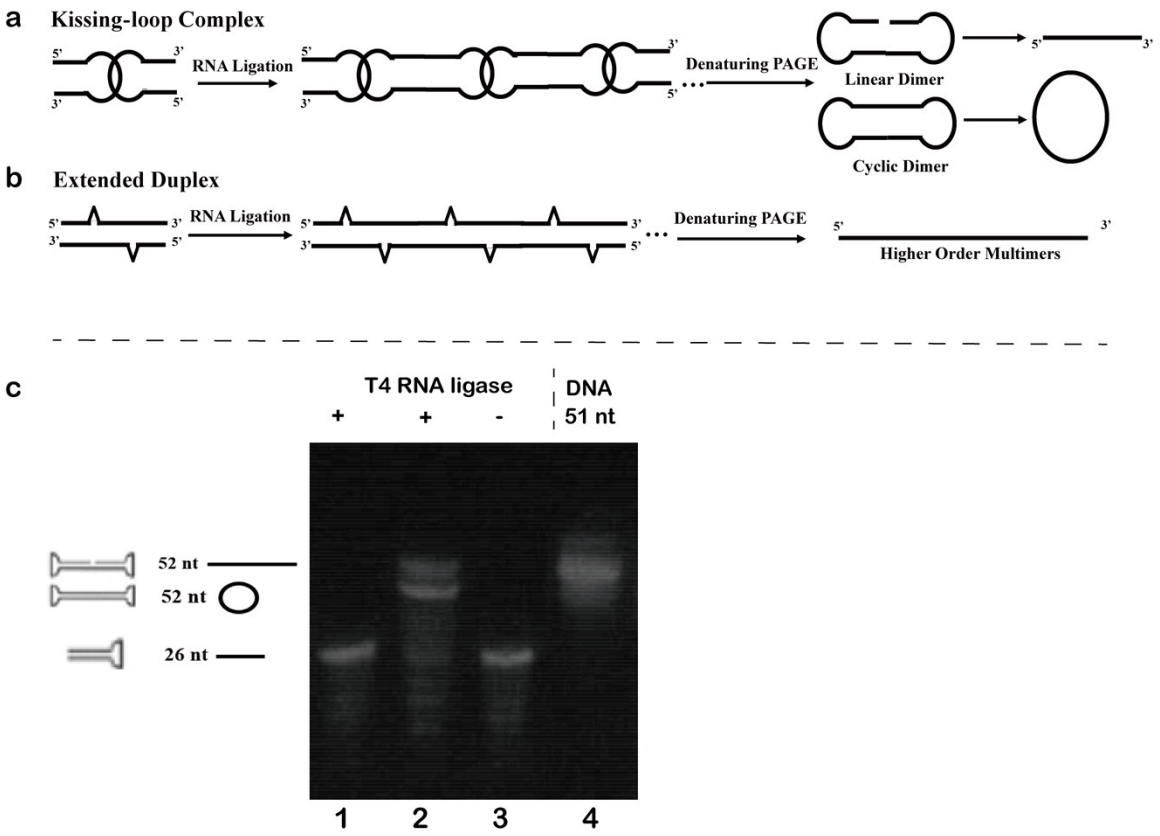

Fig. S4 Schematic presentation of the T4 RNA ligation reaction that distinguishes the kissing-loop structure from the extended duplex structure. A kissing-loop and an extended duplex produce different products that can be distinguished by denaturing PAGE. a) In the kissing loop structure case, the end product is a cyclic dimer, in which two individual hairpins have been ligated together, and a linear dimer, so only one ligation reaction could occur. b) An extended duplex yields high order multimers. c) 16% denaturing PAGE with a loading sample. From the left to the right, the samples are monomeric DIS-HIV-1 in solution (Lane1), DIS-HIV-1 dimers after an RNA ligation reaction using T4 RNA ligase (Lane 2), DIS-HIV-1 dimers without T4 RNA ligase, transforming into monomeric RNA under denaturing condition (Lane 3), and a 51-nt double strand DNA sample (Lane 4). Lanes 3 and 4 show the control experiments.

Verification of the kissing-loop structure of DIS-HIV-1 using FRET

Fluorescence resonance energy transfer (FRET) experiments were carried out using synthesized DIS-HIV-1 modified with the FRET donor Cy3 at the 3′ end and the FRET acceptor Cy5 at the 5′ end (RNA samples purchased from GenePharma Co., Ltd., Shanghai, China). 3′-Cy3-modified DIS-HIV-1 RNA and 5′-Cy5-modified DIS-HIV-1 RNA were used as control samples to verify the occurrence of FRET on the 5'-Cy5, 3'-Cy3-modified DIS-HIV-1 RNA samples. The concentrations were quantified by OD_{260} according to their individual absorption coefficients. Fluorescence spectra from 550 to 750 nm were recorded in 1-nm steps using a Hitachi F4500 Spectrofluorometer (Hitachi, Japan) with an excitation of 540 nm. All of the samples were prepared at 500 nM with the same volume of 300 μL and the results of three replicate experiments were averaged.

The fluorescence intensity of Cy3 decreased (at 560 nm), whereas that of Cy5 increased (at 660 nm) for the 500 nM FRET-pair labeled DIS-HIV-1 (Fig. S5, purple line) relative to the equal concentration of 3′-Cy3-modified DIS-HIV-1 (Fig. S5, red line) and 5′-Cy5-modified DIS-HIV-1 (Fig. S5, green line), indicating the occurrence of FRET on the 5′-Cy5, 3′-Cy3-modified DIS-HIV-1. When an equal amount of non-fluorescent labeled DIS-HIV-1 RNA was added to the 500 nM FRET-pair labeled RNA sample, which was then annealed to form dimers, no significant changes in the fluorescence intensity of Cy3 and Cy5 were observed (Fig. S5, blue line). This result excluded the possibility that the DIS-HIV-1 formed an extended duplex structure and suggested that it adopted a kissing-loop structure.

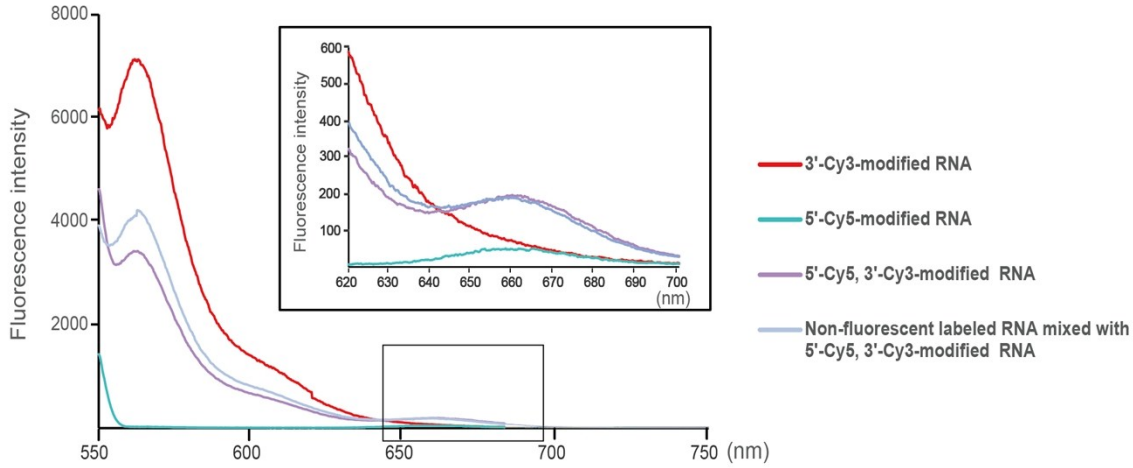

Fig. S5 Fluorescence emission spectra of fluorophore-labeled RNA samples. The fluorescence intensity of the Cy3 and Cy5 on the FRET-pair labeled RNA remained almost unchanged after adding equal amounts of non-fluorescent labeled DIS-HIV-1 RNA, indicating the kissing-loop dimeric form preference of the DIS-HIV-1.

SSNMR Characterization of DIS-HIV-1

Nucleotide-type resonance assignments

Following the characteristic ^{15}N chemical shifts of nucleotides in RNA (http://www.bmrb.wisc.edu/ref_info/statful_rna.htm), nucleotide type specific assignments were performed using the 1D HN-CP spectra of RNA with different labeling patterns. Starting from the 1D HN-CP of $(G,C)^{Lab}$-RNA with a contact time of 300 μs, the ^{15}N resonances were assigned for the amino group of G-N2 at 76 ppm, the amino group of C-N4 at 98 ppm, and the imino group of G-N1 at 147 ppm (Fig. S6 a). The 1D HN-CP spectrum of $(G,C)^{Lab}$-RNA with a mixing time of 2 ms allowed us to unambiguously assign

all of the other ^{15}N resonances, including G-N7 at 230 ppm, G-N9 at 174 ppm, G-N3 at 160 ppm, C-N1 at 150 ppm, and C-N3 at 194 ppm (Fig. S6 b).

Compared to the (G,C)^{Lab}-RNA, two more ^{15}N resonances were assigned on the HN-CP spectrum of the (G,C,A,U)^{Lab}-RNA with a short mixing time (Fig. S6 c): the imino group of U-N3 at 160 ppm and the amino group of A-N6 at 80 ppm. Further, with a CP contact time of 2 ms, the HN-CP spectrum of (C,G,A,U)^{Lab}-RNA identified the A-N1, A-N7, and A-N3, all of which have a ^{15}N chemical shift higher than 190 ppm, according to the chemical shift of δ(A-N7)> δ(A-N1)> δ(A-N3). U-N3, A-N9, and U-N1 could not be unambiguously assigned, and they may overlap with G-N3, G-N9, and C-N1.

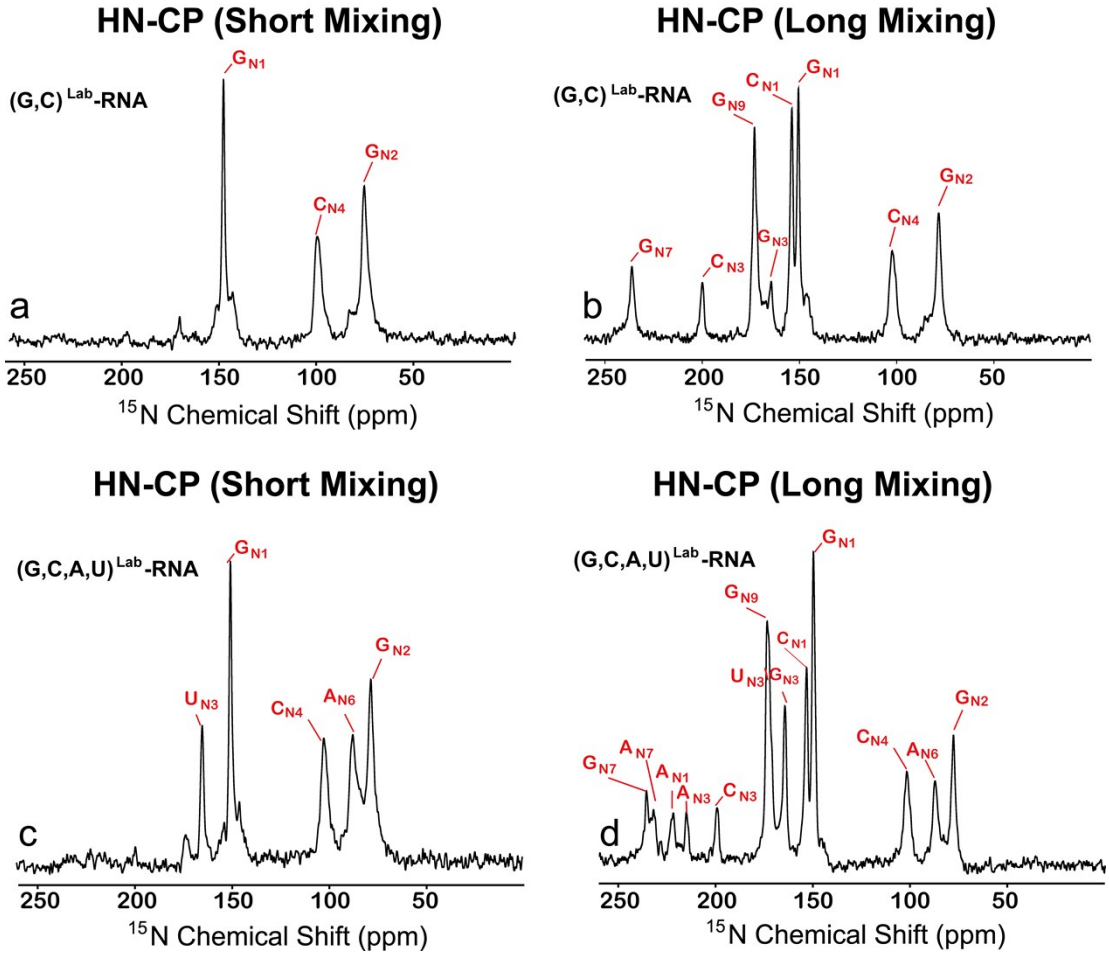

Fig. S6 1D ^{1}H-^{15}N CP spectra of (G,C)^{Lab}-RNA with CP contact times of a) 300 μs and b) 2 ms. 1D ^{1}H-^{15}N CP spectra of (G,C,A,U)^{Lab}-RNA with CP contact times of c) 300 μs and d) 2 ms. All of the spectra were acquired on a 600 MHz spectrometer with a spinning rate of 40 kHz. The nucleotide-type ^{15}N specific assignments are labeled in red.

Resolution of ^{1}H-detected SSNMR spectra

It was expected that the 1D ^{1}H SSNMR spectra of micro-crystallized RNA would have high spectral quality under a fast MAS spinning frequency, as it effectively suppresses proton-proton dipolar couplings. The experiments, shown in Fig. S7, demonstrated the progressive

decrease in proton line width with an increase in spinning rate, which gave the best spectral quality at 40 kHz MAS.

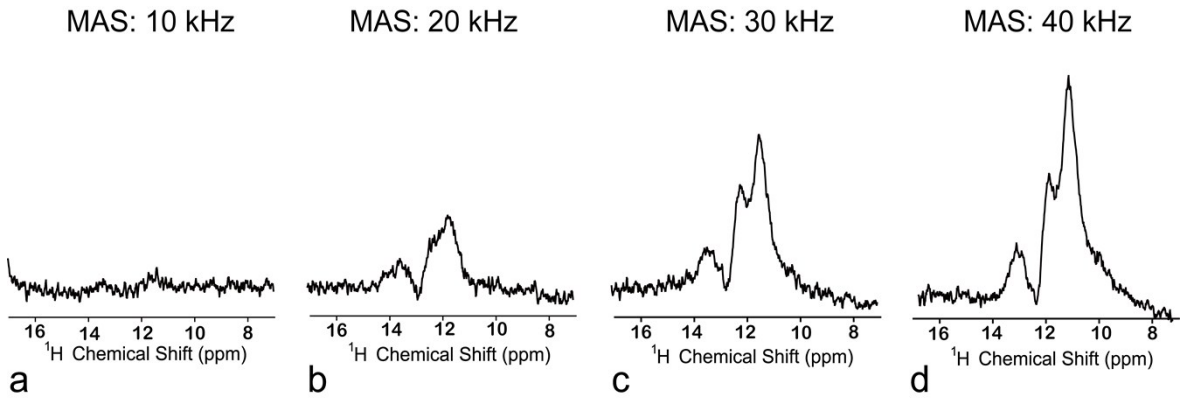

Fig. S7 1D ^{1}H-SSNMR spectra of RNA under different MAS spinning rates.

To investigate the spectral resolution of the 2D experiments, the ^{1}H-^{15}N correlation spectra at 40 kHz MAS were acquired on the (G,C)^{Lab}-RNA, (G,C,A,U)^{Lab}-RNA samples. The resonances corresponding to the imino groups of guanosines appeared in the region of the ^{15}N chemical shifts ranging from 145-150 ppm, and of the ^{1}H chemical shifts ranging from 12.0-14.0 ppm, whereas the imino groups of uridines were detected at the ^{15}N chemical shift of 163 ppm and the ^{1}H chemical shift of 14 ppm. The proton line width of the imino groups were measured to be ~500 Hz, similar to those of the amide protons of full-protonated crystallized proteins under the same spinning frequency.[11] In addition, the imino coherence lifetime, T_2' value of ^{1}H was 0.75 ms, corresponding to homogeneous proton line width of approximately 420 Hz, which suggested that inhomogeneous line width was ~80 Hz.

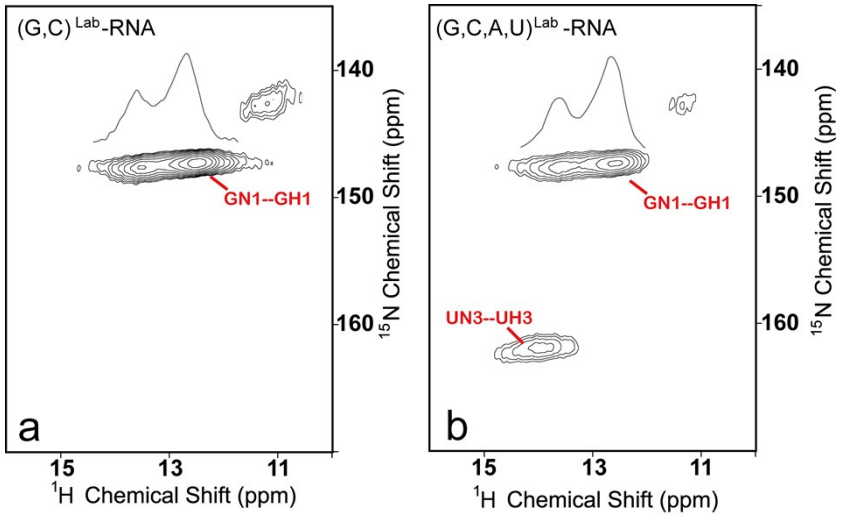

Fig. S8 2D ^{1}H-^{15}N correlation SSNMR spectra collected on a) (G,C)^{Lab}-RNA and b) (G,C,A,U)^{Lab}-RNA. The spectra are displayed for the regions of imino groups. The imino group of guanosines and uridines are marked in red. The 1D trances extracted at the ^{15}N chemical shift of 147 ppm are shown on the 2D spectra.

Inter-nucleotide polarization transfer using the ^{15}N-^{15}N PAR mechanism

We simulated the ^{15}N-^{15}N PAR transfer efficiency using the SIMPSON program.[12] The simulation was performed on a three spins system, composed of two ^{15}N spins and one ^{1}H spin (N1-H···N3), mimicking the geometry of the CG Watson-Crick base pair in RNA. The three spins were set with a linear structure. The dipolar coupling between the H and the N1 was 12 kHz, while the dipolar coupling between the H and the N3 was 1.5 kHz.

To simulate the ^{15}N-^{15}N PAR transfer for the stacked nucleotide, the structure of the sequential CG was used. The three spins were set as a triangle structure with inter-atom distances as shown in Fig. S9. The result of simulation indicated that there is no any region showing significant ^{15}N-^{15}N PAR transfers.

It is worth noting that the ^{15}N-^{15}N PAR transfer mechanism depends on geometry of the three spins system, rather than the ^{15}N-^{15}N distances. The position of proton within the three spins system (N1, H and N3) is critical to the ^{15}N-^{15}N PAR transfer efficiency.[6] In the system investigated here, higher ^{15}N-^{15}N PAR transfer efficiency was expected to those with shorter H-N3 distance. The distance between H and N3 in N1-H…N3 H-bonds within Watson-Crick GC pairs is 1.9 Å, which is much shorter than that in stacked GC pair of 3.4 Å. Correspondingly, the ^{1}H-^{15}N dipolar coupling between spin pairs of H and N3 within the Watson-Crick GC pairs and the stacked GC pairs are ~1.5 kHz and ~300 Hz, respectively. Thus it is expected that the PAR transfer would be efficient in N1-H…N3 H-bonds within Watson-Crick base pairs, but largely suppressed in stacked GC pairs, which agreed with the numerical simulations.

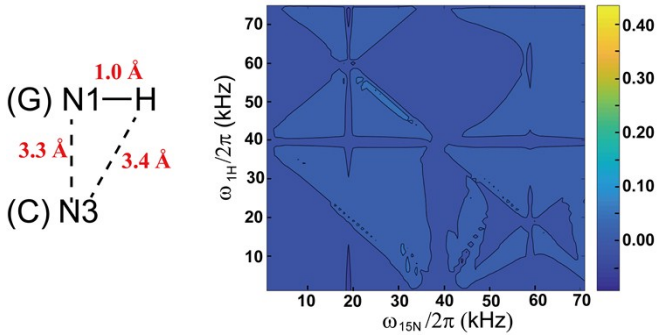

Fig. S9 Numerical simulation of PAR transfer for stacked nucleotides. The simulation was performed using the SIMPSON programs. The parameters are ω_{1H} = 600 MHz, $\omega_r/2\pi$ = 40 kHz and 7 ms PAR contact time. The geometry used in the simulation is shown on the left with inter-nuclei distantces highlighted in red.

For simulations, a crystal file ("rep256") with 256 different orientations given by the “REPULSON” algorithm and 10 gamma angles were used for powder averaging. The spin

rate of 40 kHz and the proton frequency of 600 MHz were set as experimental conditions. The carrier frequencies of N1 and N3 were set to 150 and 190 ppm, respectively. Chemical shifts anisotropy values were taken from the previous reports.[13] RF strength for the proton and the ^{15}N were scanned from 0 to 75 kHz and 0 to 72 kHz, respectively, at a step of 1 kHz. The initial magnetization was on the N1, while the final magnetization after PAR mixing is detected for the N3.

To test the ^{15}N-^{15}N PAR transfer, 1D hN(PAR)N experiments were collected on the $(G,C)^{Lab}$-RNA and $(G,C,A,U)^{Lab}$-RNA, with an ^{15}N-^{15}N PAR mixing time of 7 ms and constant spin lock fields on ^{15}N at 26 kHz and on ^{1}H at 67 kHz. A comparison of the HN-CP and the hN(PAR)N spectra revealed additional C-N3 and A-N1 resonances on hN(PAR)N, with respect to the HN-CP spectrum (Fig. S10). These two ^{15}N nuclei are acceptors of the N-H···N H-bonds of Watson-Crick base pairs, suggesting that ^{15}N-^{15}N magnetic transfer are conducted via the H-bonds. To investigate the PAR transfer efficiency, we compared the intensities of the C-N3 resonances on the hN(PAR)N spectrum with the G-N1 resonances on HN-CP, and the intensities of A-N1 of hN(PAR)N with the U-N3 resonances on the HN-CP, yielded a transfer efficiency of ~25%.

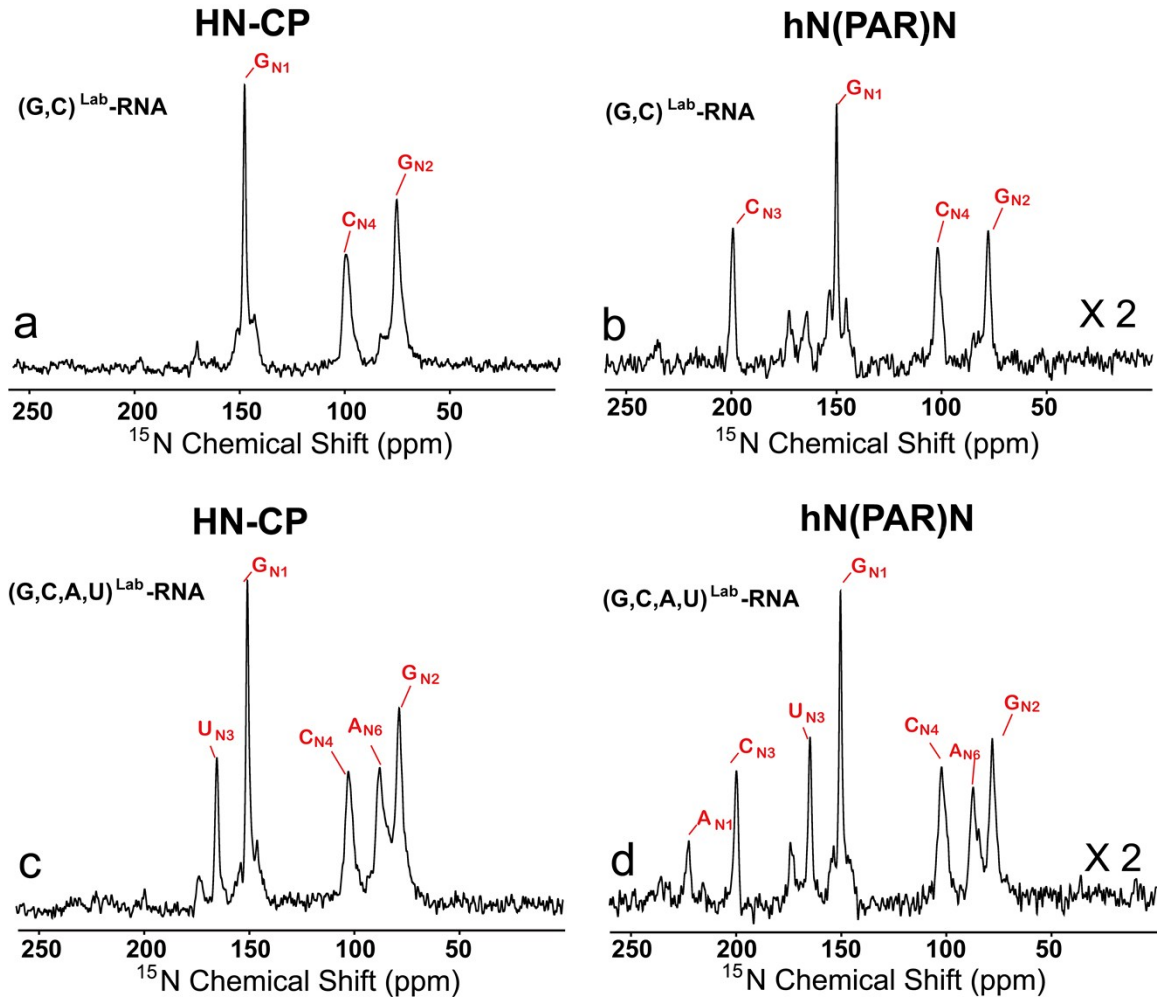

Fig. S10 Comparison of the ^{1}H-^{15}N CP and hN(PAR)N spectra of ^{15}N,^{13}C-labeled RNA. a) 1D ^{1}H-^{15}N CP and b) hN(PAR)N spectra of $(G,C)^{Lab}$-RNA. c) 1D ^{1}H-^{15}N CP and d) hN(PAR)N spectra of $(G,C,A,U)^{Lab}$-RNA. The spectra were acquired on a 600 MHz spectrometer with a MAS spinning rate of 40 kHz. The ^{15}N nucleotide-type specific assignments are labeled in red.

The 2D hNH and hN(PAR)NH spectra were also collected on the $(G,C)^{Lab}$-RNA and $(G,C,A,U)^{Lab}$-RNA samples, using the pulse sequences shown in Fig. S3. Inter-nucleotide correlations corresponding to G-H1/C-N3 were observed in the $(G,C)^{Lab}$-RNA, whereas both G-H1/C-N3 and U-H3/A-N1 were detected on the hN(PAR)NH spectra of the $(G,C,A,U)^{Lab}$-RNA (Fig. S11). These results confirmed that ^{15}N-^{15}N PAR effectively manipulates the magnetization transfer between the ^{15}N nuclei of the N-H···N H-bonds. In addition, the G-H1/C-N4 were also detected on the hN(PAR)NH spectra of both samples, further confirming the inter-nucleotide correlations. hCNH and hCN(PAR)NH were also collected on both samples, supporting the conclusions given in the manuscript.

To investigate whether the direct ^{15}N-^{1}H transfer can be used to study inter-nucleotide correlations, the ^{1}H-^{15}N spectra on $(G,C)^{Lab}$-RNA were collected with an NH-CP contact time of 2 ms. As shown in Fig. S11, no inter-nucleotide correlations representing the G-

H1/C-N3 were observed. This result suggested that the truncation effects limited remote N-H transfer, thus indicating that ^{15}N-^{15}N PAR transfer is necessary for detecting inter-nucleotide H-bonds.

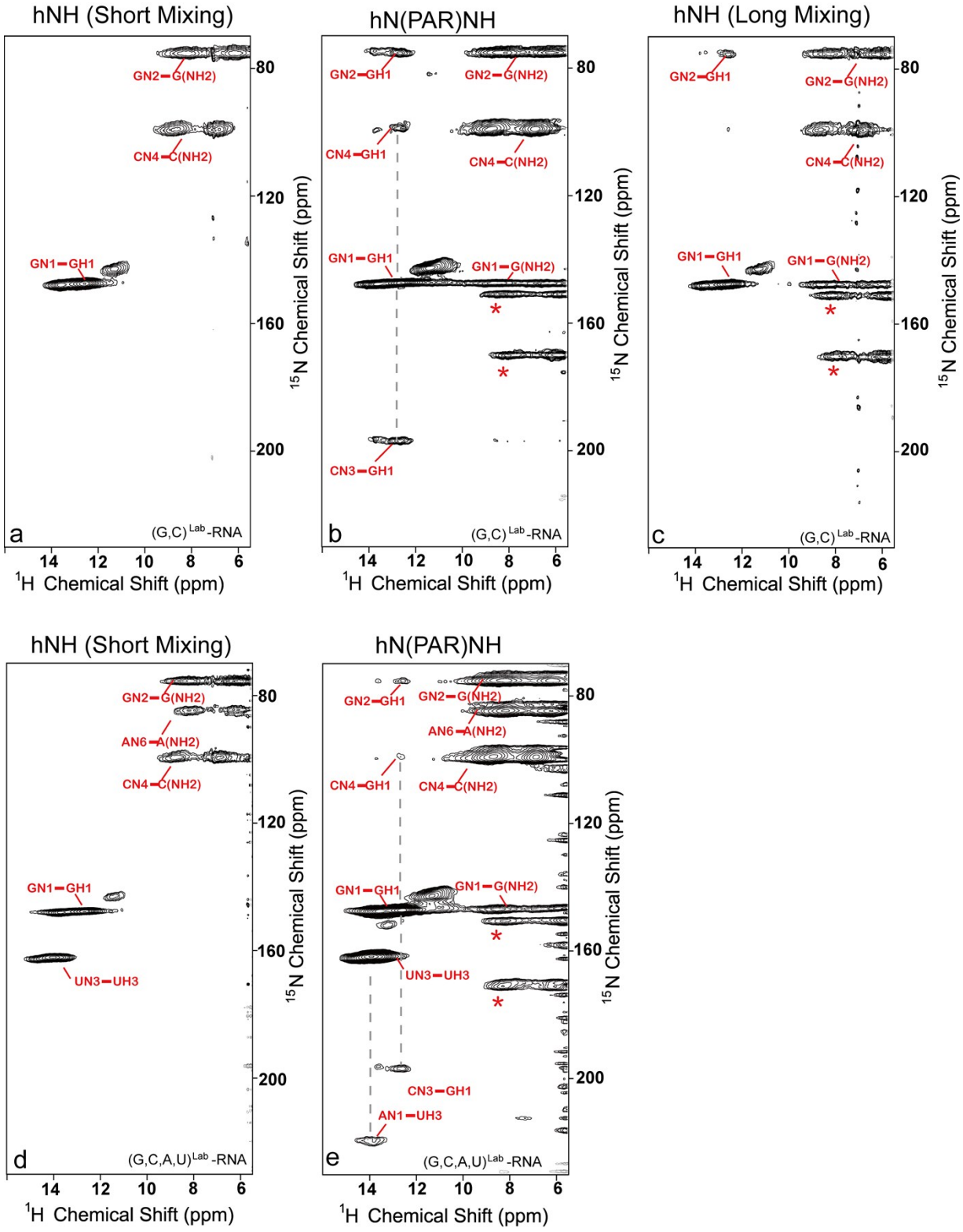

Fig. S11 Comparison of 2D hNH and 2D hN(PAR)NH spectra collected on ^{15}N,^{13}C-RNA. 2D spectra collected on (G,C)^{Lab}-RNA, including a) hNH with ^{15}N-^{1}H CP contact time of 300 μs, b) 2D hN(PAR)NH, and c) 2D hNH with ^{15}N-^{1}H CP contact time of 2 ms. 2D spectra collected on

(G,C,A,U)^{Lab}-RNA, including d) hNH with ^{15}N-^{1}H CP contact time of 300 μs and e) hCN(PAR)NH spectra. The nucleotide-type specific assignments are highlighted for the corresponding resonances. The gray dashed lines link the inter-nucleotide correlations. The asterisks mark ambiguous cross peaks. Those ambiguous cross peaks may present the correlations corresponding to hydrogen atoms in the ribose rings with C-N1/G-N9 (b,e), or hydrogen atoms with U-N1/A-N9 (e).

Distinguishing the Kissing-loop Structure from the Extended Duplex Structure of RNA Using SSNMR

DIS-HIV-1 forms a kissing-loop structure in solution, as proven by the T4 RNA ligation and FRET experiments (Fig. S4 and S5). However, in crystals the architecture of dimeric DIS-HIV-1 is unknown. We addressed this issue by using an isotopically diluted sample, di-(G,C)^{Lab}-RNA, which was prepared by mixing equal amounts of (G,C)^{Lab}-RNA and NA-RNA followed by annealing.

In such a mixture, the labeling patterns for the ^{15}N site of NH···N H-bonds within the base pairs could be either kissing-loop structures or extended duplex structures. For the kissing-loop structure, 50% of the hairpins would have Watson-Crick base pairs with ^{15}NH···^{15}N patterns, and the other 50% would be unlabeled. In this case, the ^{15}N-^{15}N PAR transfer yield would not be affected (Fig. S12). In contrast, in an extended duplex, 25% of the duplexes would have base pairs with ^{15}NH···^{15}N patterns, but 50% of the duplexes would have base pairs with ^{15}NH···^{14}N or ^{14}NH···^{15}N patterns. These patterns would not affect the ^{1}H-^{15}N correlations, but would largely suppress the ^{15}N-^{15}N PAR transfer, leading to much lower PAR transfer efficiency.

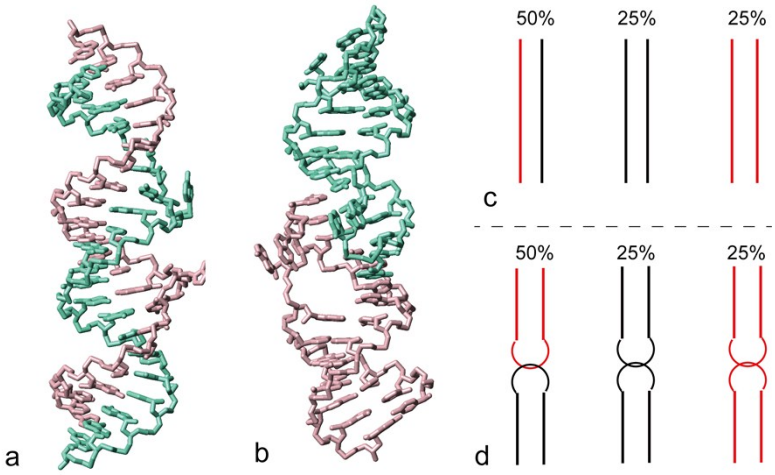

Fig. S12 Representative structures of DIS-HIV-1 and schematic representation of the relative population of labeling patterns for RNA dimers in a 1:1 mixture of isotope-labeled RNA and unlabeled RNA. a) An extended duplex structure of DIS-HIV-1 (PDB code: 1Y99). b) A kissing-loop conformation of DIS-HIV-1 (PDB code: 2B8S). The different monomers are shown in pink and light green, respectively. c) Population of labeling patterns for RNA duplexes in a 1:1 mixture of isotope-labeled RNA and unlabeled RNA. The black and red lines represent the unlabeled and ^{15}N,^{13}C-

labeled monomer, respectively. ^{15}N-^{15}N PAR transfer along the H-bonds within the Watson-Crick base pairs would only occur through the duplex formed by two isotope-labeled monomers (the right). d) Population of labeling patterns for kissing-loop structure in a 1:1 mixture of isotope-labeled RNA and unlabeled RNA. The colors indicate the labeling scheme as the same as that in c). Within the kissing-loops, the ^{15}N-^{15}N PAR would effectively polarize the ^{15}N magnetization through the H-bonds of the Watson-Crick base pairs within the same hairpin (the left and the right).

To test this, 1D hN(PAR)N experiments were conducted on the di-(G,C)^{Lab}-RNA and the undiluted (G,C)^{Lab}-RNA. The ^{15}N-^{15}N PAR transfer yields were measured for both samples by comparing the intensities of C-N3 on hN(PAR)N and G-N1 on hN-CP, resulting in a yield of 25% and 21% for the undiluted and the diluted samples, respectively (Fig. S13). These results suggested that the PAR transfer efficiency was not significantly affected by the isotopic dilution, demonstrating the kissing-loop architecture of DIS-HIV-1 rather than the duplex structure. Similarly, 2D hCN(PAR)NH were collected from both the diluted and undiluted samples, both of which displayed resonances corresponding to the characteristic spectral patterns of NH···N H-bonds within the CG base pairs (Fig. 3 of the manuscript and S14). The relative intensities between the cross peaks of the inter- and the intra-nucleotide correlations were close in both samples, further confirming the kissing-loop structure of dimeric DIS-HIV-1. Therefore, the architecture of DIS-HIV-1 in crystals was the same as that in solution.

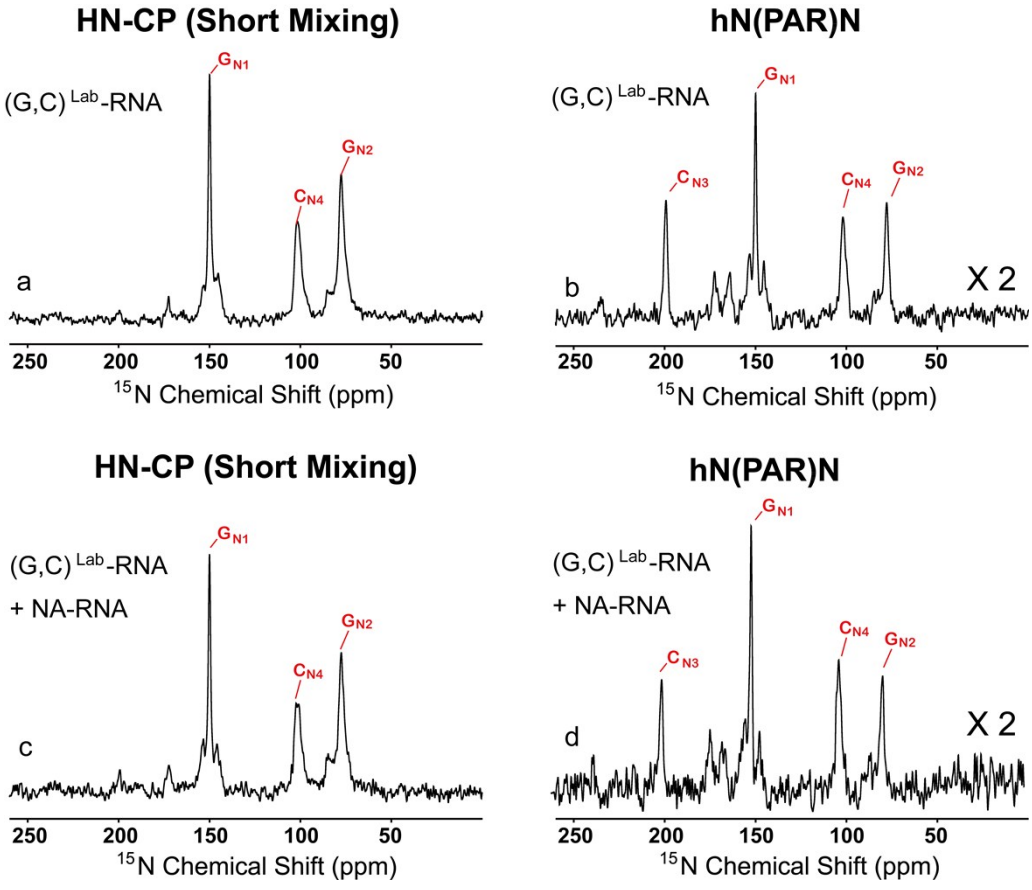

Fig. S13 a) 1D ^{1}H-^{15}N CP and b) hN(PAR)N spectra of (G,C)^{Lab}-RNA. c) 1D ^{1}H-^{15}N CP and d) hN(PAR)N spectra of di-(G,C)^{Lab}-RNA.

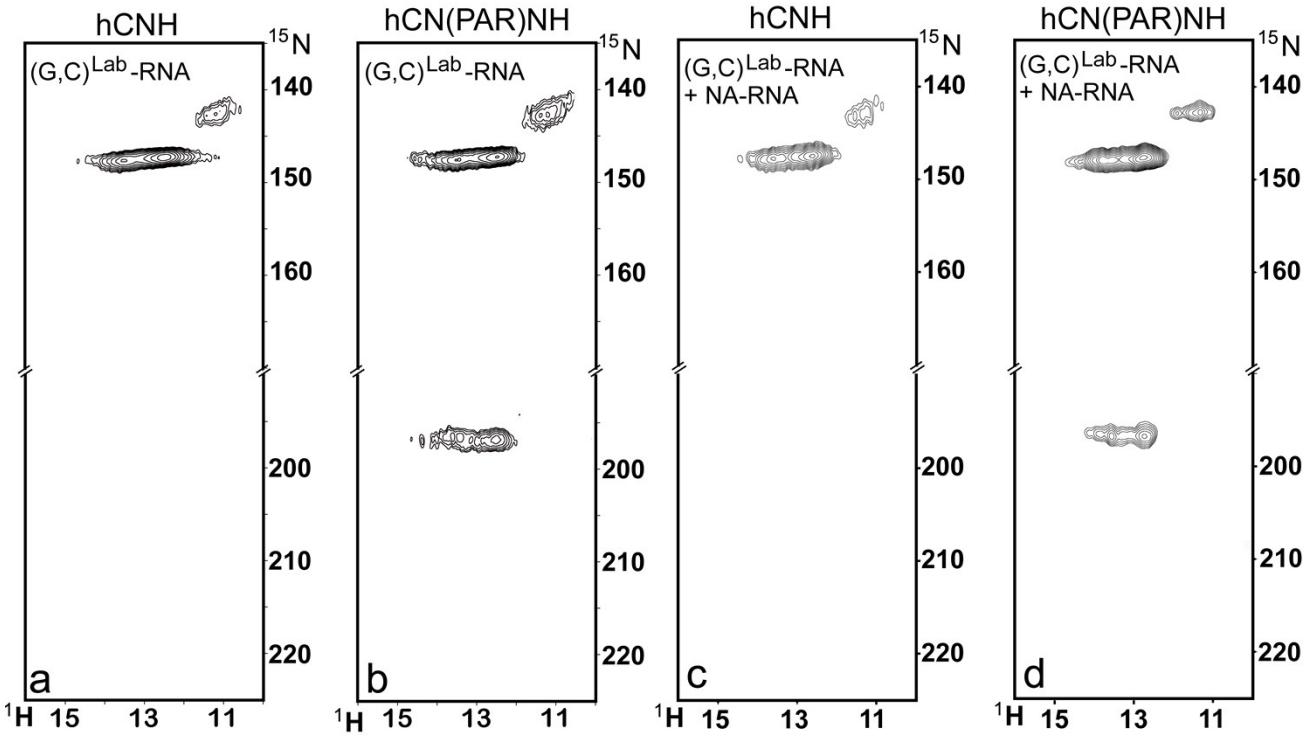

Fig. S14 a,b) The 2D hCNH and the 2D hCN(PAR)NH spectra of (G,C)^{Lab}-RNA. c,d) The 2D hCNH and the 2D hCN(PAR)NH spectra of (G,C)^{Lab}-RNA mixed with NA-RNA in an equal molar ratio.

References

1 J. F. Milligan, D. R. Groebe, G. W. Witherell and O. C. Uhlenbeck, *Nucleic Acids Res.,* 1987, **15,** 8783-8798.
2 R. W. Martin and K. W. Zilm, *J. Magn. Reson.,* 2003, **165,** 162-174.
3 K. Sharma, P. K. Madhu and V. Agarwal, *J. Magn. Reson.,* 2016, **270,** 136-141.
4 D. H. Zhou and C. M. Rienstra, *J. Magn. Reson.,* 2008, **192,** 167-172.
5 S. R. Hartmann and E. L. Hahn, *Phys. Rev.,* 1962, **128,** 2042-2053.
6 (a) G. De Paepe, J. R. Lewandowski, A. Loquet, A. Bockmann and R. G. Griffin, *J. Chem. Phys.,* 2008, **129,** 1-21; (b) J. R. Lewandowski, G. De Paepe, M. T. Eddy, J. Struppe, W. Maas and R. G. Griffin, *J. Phys. Chem. B,* 2009, **113,** 9062-9069; (c) J. R. Lewandowski, G. De Paepe, M. T. Eddy and R. G. Griffin, *J. Am. Chem. Soc.,* 2009, **131,** 5769-5776; (d) K. J. Donovan, R. Silvers, S. Linse and R. G. Griffin, *J. Am. Chem. Soc.,* 2017, **139,** 6518-6521.
7 M. Baldus, A. T. Petkova, J. Herzfeld and R. G. Griffin, *Mol. Phys.,* 1998, **95,** 1197-1207.
8 R. Keller, *The Computer Aided Resonance Assignment Tutorial*, CANTINA Verlag, Switerland, 2004.
9 C. R. Morcombe and K. W. Zilm, *J. Magn. Reson.,* 2003, **162,** 479-486.
10 F. Dardel, R. Marquet, C. Ehresmann, B. Ehresmann and S. Blanquet, *Nucleic Acids Res.,* 1998, **26,** 3567-3571.
11 D. H. Zhou, G. Shah, M. Cormos, C. Mullen, D. Sandoz and C. M. Rienstra, *J. Am. Chem. Soc.,* 2007, **129,** 11791-11801.
12 M. Bak, J. T. Rasmussen and N. C. Nielsen, *J. Magn. Reson.,* 2000, **147,** 296-330.
13 (a) A. Grishaev, L. Yao, J. Ying, A. Pardi and A. Bax, *J. Am. Chem. Soc.,* 2009, **131,** 9490-9491; (b) D. Stueber and D. M. Grant, *J. Am. Chem. Soc.,* 2002, **124,** 10539-10551.